





Cite this: *J. Mater. Chem. C*, 2019, 7, 12328

Utilizing the heterocyclic effect towards high contrast ratios of mechanoresponsive luminescence based on aromatic aldehydes†

Fang Zhang, Xiaozhong Liang, Da Li, Xiangkai Yin, Xia Tian, Bin Li, Hong Xu, Kunpeng Guo * and Jie Li *

A high contrast ratio is required by mechanoresponsive luminescent (MRL) materials to enable their adoption in mechanical sensors. However, the effective design principle remains restricted by the lack of understanding of the necessary features of such luminophores. In this contribution, a series of simple aromatic aldehydes, namely, **APCz**, **APAd**, **APPo**, and **APPt**, was designed and synthesized by combining different heterocyclic cores with 4-benzoyl substituted at the symmetrical positions. The heterocyclic cores *N*-butyl-carbazole (**APCz**), *N*-butyl-9,9-dimethyl acridine (**APAd**), *N*-butyl-phenoxazine (**APPo**), and *N*-butyl-phenothiazine (**APPt**) endowed the moderately twisted compounds with the ability of emitting luminescence in the solid state and in adopting metastable states in their pristine-crystal state. These features enabled phase and multicolor changes under external-force stimuli. Single-crystal analyses revealed that decreasing the type of noncovalent interactions by changing the heterocyclic cores from five- to six-membered rings with additional heteroatoms led to the formation of compounds sensitive to external force and to a dramatic increase in MRL contrast ratio from $\Delta\lambda = 10$ nm to $\Delta\lambda = 53$ nm. Overall, this work provided new insights into the design of high-contrast stimuli-responsive luminescent materials.

Received 19th August 2019,
Accepted 15th September 2019

DOI: 10.1039/c9tc04586d

rsc.li/materials-c

Introduction

The design and synthesis of mechanoresponsive luminescent (MRL) materials, which exhibit altered solid emission under mechanical force stimuli, are of considerable practical and academic interest for applications in optical devices, mechanical sensors, security paper, and disaster warning.^{1–6} In studying these materials, the origin of the MRL phenomenon, including the changes in the molecular packing and molecular conformation upon external force stimuli, has been proposed to obtain additional insights into improving their performance.^{7–10} In this context, organic MRL materials have attracted considerable attention because of their flexible molecular structure tailoring and intra/intermolecular interaction modulating.^{11–16} In principle, a material should possess the three following essential characteristics to ensure that it exhibits prominent MRL behavior.

First, a material must exhibit efficient emission in solid state.^{1–3} Second, a metastable state must be present to ensure that its properties can be changed under force stimuli.^{7,8} Third, a clear color difference should be present to meet the high contrast luminescence recording requirements.^{8–10,14}

Generally, introducing aggregation-induced emission building blocks, such as highly twisted tetraphenylethylene and triphenylamine, is an effective strategy in realizing efficient solid emission.^{7,10,17–21} For example, Tang *et al.* successfully incorporated tetraphenylethylene and triphenylamine into a variety of small molecules and polymers, which display advantages in organic light-emitting diodes, bioimaging, and MRL materials.^{5,12} Similarly, the utility of moderately and slightly twisted molecules as building blocks in organic electronics has also made them extensively studied molecules due to their relative facile synthesis and functionalization.^{22–26} However, the molecules with small steric hindrance in the condensed state tend to form compact aggregates due to π - π interactions, which increased the non-radiative path and resulted in emission quenching. To date, only a few moderately and slightly twisted molecules exhibiting MRL phenomena have been reported by mechanically disturbing their molecular packing motifs in metastable nanostructures.^{23,24,27–29} However, the lack of single-crystal analyses limits insights into their molecular features in precise designing and synthesizing

Ministry of Education Key Laboratory of Interface Science and Engineering in Advanced Materials, Research Center of Advanced Materials Science and Technology, Taiyuan University of Technology, Taiyuan 030024, China.

E-mail: guokunpeng@tyut.edu.cn, lijie01@tyut.edu.cn

† Electronic supplementary information (ESI) available: Experimental section, supplementary figures, crystallographic data. CCDC 1842477, 1847380 and 1847379. For ESI and crystallographic data in CIF or other electronic format see DOI: 10.1039/c9tc04586d

such high contrast MRL materials. Therefore, it is important to understand the necessary molecular features of high contrast MRL luminophores for increasing the dimensionality of MRL materials.

Heterocycles, which are cyclic hydrocarbons embedded with one or more heteroatoms, are well established as key building blocks in biostructures and functional materials such as luminescent materials.^{11,30–35} Heteroatoms are indispensable in achieving versatile functions because they enable variable conformations of molecules, exert electron-donating or withdrawing effects, and even induce complicated excited states.^{31,32,35} Meanwhile, given the excellent sensitivity of the intramolecular charge transfer (ICT) emission to alterations in the external environment, the development of acceptor–donor–acceptor (A–D–A)-type ICT luminophores has raised significant concerns for advanced MRL materials.^{36–38} Here, we present a strategy of imposing molecular feature screening for realizing high contrast ratios of mechanoresponsive luminescence. This strategy was inspired by the fact that the building blocks of a compound, such as donor or acceptor units, can largely affect the molecular conformation and intra/intermolecular interactions. Hence, we aimed to introduce commonly used heterocyclic rings as donors to produce mutative A–D–A luminophores with different crystal characteristics and stability in the solid state to obtain additional insights into the molecular features of MRL materials with high contrast ratios.

Symmetrical aromatic aldehydes can be regarded as a type of simple A–D–A compound that are beneficial in determining the regularity of realizing MRL behavior in donor unit adjustment. In this work, we designed and synthesized four A–D–A heterocyclic-based aromatic aldehydes with 4-formylbenzene acceptors that differed in *N*-butyl-carbazole (APCz), *N*-butyl-9,9-dimethyl acridine (APAd), *N*-butyl-phenoxazine (APPo), and *N*-butyl-phenothiazine (APPt) donors (Fig. 1) on the basis of the anticipation that the electron donative aromatic heterocyclic compounds can be effective in tuning the molecular conformation with diverse intra/inter molecular interactions and molecular packing modes. The compounds can be facilely synthesized from commercially available formyl aromatic boronic acid with different bromide aromatic rings *via* Suzuki coupling, as depicted in Scheme S1 (ESI†). Compared with the referenced

heteroatom-free aldehyde (APBz, Scheme S1, ESI†) with a 5-octylbenzene donor exhibiting nonemission and non-MRL behavior in solid state, APCz with a *N*-containing five-membered heterocycle in the donor moiety resulted in a minimal increase in molecular distortion and ICT effect, thereby emitting blue luminescence in the crystal. Although the crystal of APCz was in a metastable state, no megascopic color change was observed under grinding with the emission band shift of only 10 nm. However, APAd, APPo, and APPt showed significantly increased MRL contrast ratios accompanied with an evident color change from yellow to green, red to orange, and yellow to blue under grinding, respectively. Theoretical and single-crystal analyses revealed that after changing the heterocyclic cores from five-membered rings to six-membered rings with additional heteroatoms, the sensitivity to external force increased with decreased noncovalent interaction types. With increased molecular distortion, APPt, which exhibited a 53 nm emission band shift under grinding, showed the highest contrast ratio among the samples. Our study is significant in providing insights into the molecular features in designing MRL materials with high contrast ratios.

Results and discussion

Theoretical calculations

To explore the influence of varied heterocyclic donors on the molecular conformations and ICT characteristics of these compounds, we first evaluated the optimized molecular geometries and frontier orbital distributions by DFT calculations at the B3LYP/6-31G* level. As illustrated in Fig. 1, the dihedral angles between the phenyl ring and the central heterocyclic donors were 35°/35° for APCz, 31°/25° for APAd, 29°/29° for APPo, and 35°/40° for APPt. These results demonstrated that all four molecules adopted moderately twisted conformations. According to our previous studies, such moderately twisted conformations may result in compounds exhibiting mechanoresponsive properties in the solid state.^{23,24,36} The dihedral angle between the central phenyl core and adjacent phenyl rings for the referenced APBz was 33°/33° (Fig. S1, ESI†), which was smaller than that of APCz with a *N*-containing carbazole in the donor moiety. As a result, the introduction of a heteroatom

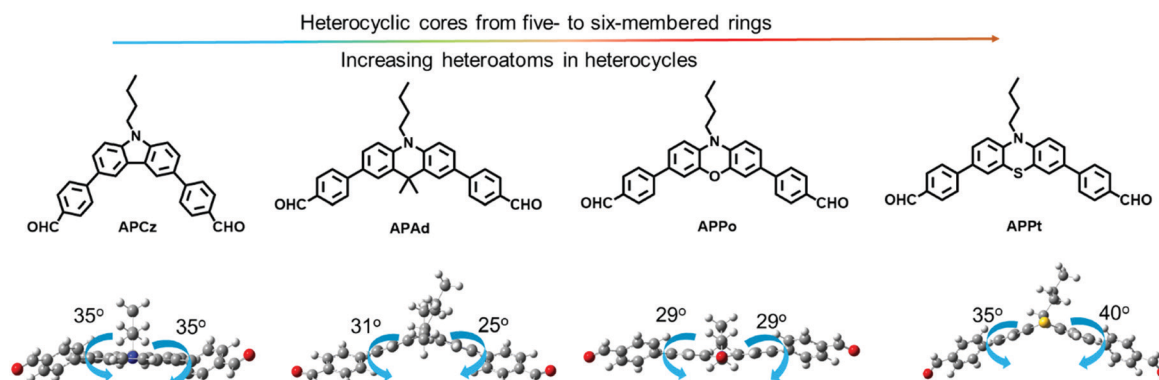


Fig. 1 Molecular structure and geometrically optimized 3D molecular models of APCz, APAd, APPo and APPt.

into the central core of A–D–A molecules may increase the molecular distortion.

As shown in Fig. S2 (ESI[†]), the spatial separation between the highest occupied molecular orbitals (HOMOs) and the lowest unoccupied molecular orbitals (LUMOs) of the referenced **APBz** was not pronounced, thereby indicating a weak ICT effect of **APBz**. However, from **APCz** to **APAd**, **APPo**, and **APPt**, the HOMOs are more concentrated on the central heterocyclic cores and the adjacent phenyl rings, although the LUMOs are primarily distributed on the formyl groups as well as the phenyl rings. These results indicated that the change in the central cores from heteroatom-free phenyl rings to heterocycles with increased ring sizes and heteroatoms would be an effective way to improve the ICT effect of the compounds.

Photophysical properties

To evaluate the ICT characteristics of the compounds further, we investigated the UV-vis absorption and photoluminescence properties of **APCz**, **APAd**, **APPo**, and **APPt**, and studied the referenced **APBz** in solvents with different polarities. The weak ICT characteristic of **APBz** was proved by the insensitivity of photophysical properties to solvent polarity change. As shown in Fig. S3 (ESI[†]), the absorption spectra of **APBz** in various solvents exhibited one characteristic absorption band in a narrow range of 288–298 nm, and nearly no observable photoluminescence was observed upon changing the solvents' polarities. After replacing the central donor core with heterocycles, the absorption maximum (λ_{abs}) of **APCz**, **APAd**, **APPo**, and **APPt** was red-shifted by approximately 18–27 nm when increasing the solvent polarity from hexane to DMSO (Fig. S4, ESI[†]). Compared with **APBz**, these red-shifts indicated a large change in dipole moment in the ground state in different solvents for **APCz**, **APAd**, **APPo**, and **APPt**. All heterocycle-based aromatic aldehydes showed significant solvatochromic effects with respect to **APBz**, as generally attributed to typical ICT effects. We found that $\Delta\lambda$, *i.e.*, the maximum peak photoluminescence (λ_{PL}) shift between emissions in the nonpolar solvent hexane and in the highly polar solvent DMSO, was 108 nm for **APCz**, 137 nm for **APAd**, 149 nm for **APPo**, and 63 nm for **APPt**, thereby leading to a distinct change in fluorescence color that can be clearly distinguished by the naked eye under a 365 nm UV lamp (Fig. 2 and Table 1).

Studies on the Lippert–Mataga equation revealed that the solvatochromic effect is related to a change in molecular dipole moment between the excited and ground states. Fig. S5 (ESI[†]) shows the plots of the Stokes shift *versus* orientational polarizability.

The plots showed one set of linearity indicative of one dominant ICT excited state maintained in solvents with different polarity. The slopes of the best-fit line, which was related to the dipole moment change between the ground state and the excited state, were 13 018, 14 750, 12 886, and 6498 for **APCz**, **APAd**, **APPo**, and **APPt**, respectively. These results suggested that the dipole moments in the excited state increased in a polar solvent when the charges transferred from the central heterocyclic donors to the peripheral withdrawing formyl groups. As a result, the polarized excited state was stabilized to adapt to the enhanced dipole

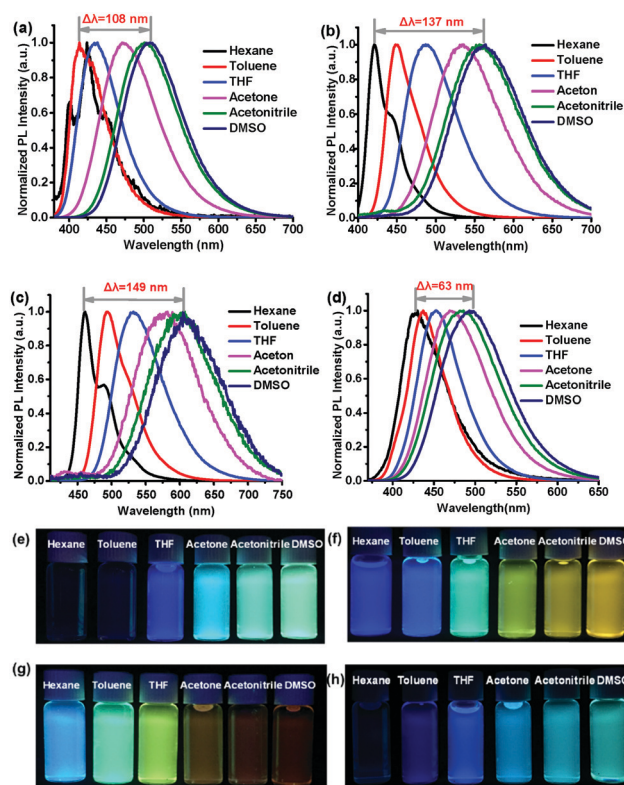


Fig. 2 Fluorescence spectra of (a) **APCz**, (b) **APAd**, (c) **APPo** and (d) **APPt** in various organic solvents (10 μM). Photographs of (e) **APCz**, (f) **APAd**, (g) **APPo** and (h) **APPt** in various solvents under UV light (365 nm).

moment by the relocation of the polar solvent molecules, thereby leading to lowered energy and red-shifted fluorescence and showing that **APCz**, **APAd**, **APPo**, and **APPt** are highly sensitive to solvent polarity.

Thermal stability characterization

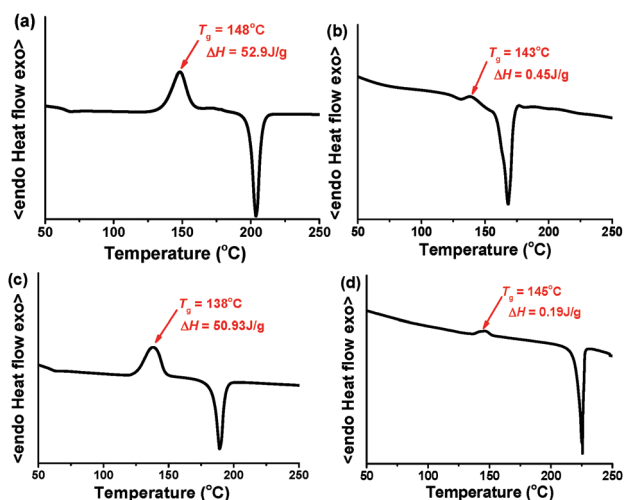
To understand the difference of the thermal stability between the various molecular structures, we performed differential scanning calorimetry measurements. As shown in Fig. 3, the pristine powders of **APCz**, **APAd**, **APPo** and **APPt** all displayed a phase transition peak prior to their melting points, respectively. The corresponding exothermal peaks were observed at approximately 148 $^{\circ}\text{C}$ ($\Delta H = 52.9 \text{ J g}^{-1}$) for **APCz**, 143 $^{\circ}\text{C}$ ($\Delta H = 0.45 \text{ J g}^{-1}$) for **APAd**, 138 $^{\circ}\text{C}$ ($\Delta H = 50.93 \text{ J g}^{-1}$) for **APPo**, and 145 $^{\circ}\text{C}$ ($\Delta H = 0.19 \text{ J g}^{-1}$) for **APPt**, thereby indicating that the four heterocyclic aromatic aldehydes were present in a metastable state. By contrast, without hetero atoms in the central core, the reference **APBz** pristine powder only exhibited one exothermal peak at 94.4 $^{\circ}\text{C}$ ($\Delta H = 74.27 \text{ J g}^{-1}$) corresponding to its melting point (Fig. S6, ESI[†]). These results suggested that the introduction of heterocycles was beneficial, thereby inducing the aromatic aldehydes to form metastable states in their pristine powders and leading to the possibility of yielding MRL behavior under external force stimuli.

Mechanoresponsive luminescence properties

Taking their moderately twisted molecular conformations and metastable states in pristine crystals together, MRL behavior

Table 1 Photophysical properties of **APBz**, **APCz**, **APAd**, **APPo** and **APPt** in various solvents

Compounds	Solvent	Δf	λ_{Abs} (nm)	ϵ ($10^4 \text{ M}^{-1} \text{ cm}^{-1}$)	λ_{PL} (nm)	Stokes shift (cm^{-1})	Φ_{F} (%)
APBz	Hexane	0	288	5.689	—	—	—
	Toluene	0.012	289	4.782	—	—	—
	THF	0.21	294	6.411	—	—	—
	Acetone	0.28	295	5.485	—	—	—
	Acetonitrile	0.29	295	6.855	—	—	—
	DMSO	0.26	298	8.215	—	—	—
APCz	Hexane	0	350	4.689	400	3571	0.7
	Toluene	0.012	355	4.489	413	3956	2.9
	THF	0.21	358	4.948	435	4944	34.7
	Acetone	0.28	356	4.737	473	6948	35.2
	Acetonitrile	0.29	359	4.767	502	7935	39.9
	DMSO	0.26	368	4.957	508	7489	39.0
APAd	Hexane	0	383	4.425	421	3937	34.0
	Toluene	0.012	393	4.287	449	4568	29.6
	THF	0.21	395	4.192	489	6049	17.6
	Acetone	0.28	396	4.499	534	7522	15.8
	Acetonitrile	0.29	394	4.292	556	8316	12.3
	DMSO	0.26	408	4.328	558	7503	10.4
APPo	Hexane	0	414	2.443	461	2463	2.8
	Toluene	0.012	429	2.43	494	3067	51.1
	THF	0.21	432	2.26	532	4351	23.9
	Acetone	0.28	427	2.297	580	6178	2.6
	Acetonitrile	0.29	429	2.476	600	6643	1.4
	DMSO	0.26	441	2.374	610	6282	1.0
APPt	Hexane	0	358	2.954	429	4623	5.4
	Toluene	0.012	367	5.532	436	4312	20.3
	THF	0.21	372	6.073	452	4758	42.6
	Acetone	0.28	365	6.458	470	6121	44.9
	Acetonitrile	0.29	365	6.259	482	6650	44.3
	DMSO	0.26	376	6.25	492	6271	37.0

**Fig. 3** DSC curves of compounds (a) **APCz**, (b) **APAd**, (c) **APPo** and (d) **APPt** in the pristine state.

was anticipated for **APCz**, **APAd**, **APPo**, and **APPt**. To verify our speculation, we spread the pristine powders of the four heterocyclic aromatic aldehydes with different patterns on filter paper and recorded the changes in their fluorescence characteristics

under mechanical grinding, and the corresponding parameters are collected in Table 2. The original blue fluorescence of **APCz** was almost maintained after grinding (Fig. 4), although a blue shift of 10 nm from 474 nm to 464 nm was observed, and an increased absolute fluorescence quantum yield (Φ_{F}) from 3.4% to 53.6% was recorded (Fig. 5a and Table 2). These results indicated an extremely low MRL contrast ratio of **APCz**. When replacing the centered five-membered ring *N*-butyl-carbazole in **APCz** with a six-membered ring *N*-butyl-9,9-dimethyl acridine, the resulting **APAd** exhibited a yellow emission ($\lambda_{\text{PL}} = 558 \text{ nm}$ and $\Phi_{\text{F}} = 11.7\%$) in its pristine powder and an enhanced green emission ($\lambda_{\text{PL}} = 514 \text{ nm}$ and $\Phi_{\text{F}} = 64.1\%$) after grinding (Fig. 4, 5b, and Table 2). Compared with **APCz**, the spectral shift of 44 nm and distinct fluorescence color change of **APAd** observable by naked eyes indicated an evidently improved MRL contrast ratio. The further improvement of the MRL contrast ratio was observed with increased heteroatoms in the centered moiety. The application of mechanical grinding to the pristine **APPo** powder resulted in a blue shift of 48 nm from 621 nm to 573 nm and increased Φ_{F} from 9.37% to 36.2% (Fig. 5c and Table 2). This process was accompanied by a distinct fluorescence color change from red to orange (Fig. 4). The largest MRL contrast ratio with a blue shift of 53 nm from 527 nm ($\Phi_{\text{F}} = 7.43\%$) to 474 nm ($\Phi_{\text{F}} = 68.7\%$) was observed upon mechanical grinding of the **APPt** powder, accompanied by a remarkable fluorescence color change and enhancement from yellow to blue (Fig. 4). The diversity of the MRL contrast ratio of the four compounds can be further demonstrated in the Commission Internationale de l'Eclairage (CIE) diagram to show their different sensitivity to mechanical force. As shown in Fig. S7a (ESI[†]), the CIE color coordinates of **APCz** changed from (0.18, 0.24) to (0.15, 0.20) after grinding, which still located in the blue color zone. However, in the case of **APPt**, a considerable change from the yellow-green color zone (0.34, 0.60) to the blue color zone (0.16, 0.26) was realized upon grinding. **APPt** exhibited an excellent MRL contrast ratio. However, insignificant emission in the pristine powders and mechanical grinding did not lead to any change in the fluorescence of **APBz**, which can be attributed to its low distorted molecular conformation, weak ICT effect, and thermal stability in the solid state. On the basis of these results, we can conclude that the characteristics of centered heterocyclic rings can regulate the fluorescence color and the MRL contrast ratio of compounds significantly.

MRL mechanism study

To investigate the mechanism of the MRL behavior, we recorded X-ray diffraction (XRD) patterns and time-resolved spectra. As shown in Fig. 6a–d, the pristine powders of **APCz**, **APAd**, **APPo**, and **APPt** showed many sharp and strong diffraction peaks, thereby suggesting typical crystalline characteristics. In the wide angle region, the peaks were observed at approximately 25° , which were primarily caused by intermolecular interactions, such as π - π and C-H $\cdots\pi$. These noncovalent interactions between adjacent aromatic molecules often result in decreased or quenched emission in the solid state, thereby accounting for

Table 2 Photophysical properties of APCz, APAd, APPo and APpt in pristine and ground solid states

Compounds	Pristine sample					Ground sample				
	λ_{PL} (nm)	Φ_{F} (%)	τ (ns)	k_{r} (ns^{-1})	k_{nr} (ns^{-1})	λ_{PL} (nm)	Φ_{F} (%)	τ (ns)	k_{r} (ns^{-1})	k_{nr} (ns^{-1})
APCz	474	3.4	4.28	0.0079	0.2257	464	53.6	5.56	0.0965	0.0835
APAd	558	11.7	13.72	0.0012	0.0716	514	64.1	15.94	0.0402	0.0225
APPo	621	9.37	2.53	0.0071	0.3881	573	36.2	4.46	0.0812	0.1431
APPt	527	7.43	3.92	0.0031	0.2521	474	68.7	5.31	0.1295	0.0590

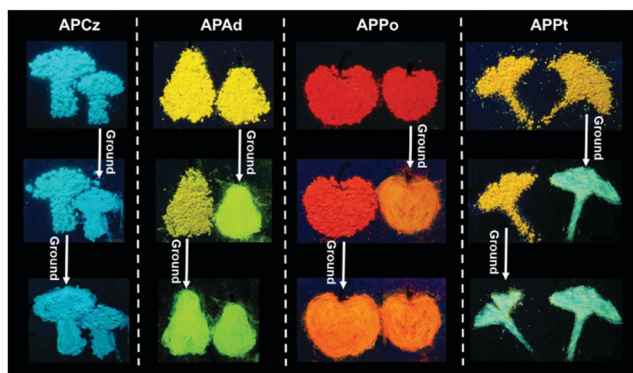


Fig. 4 Photographs of APCz, APAd, APPo and APpt before and after mechanical grinding performed under a 365 nm UV lamp.

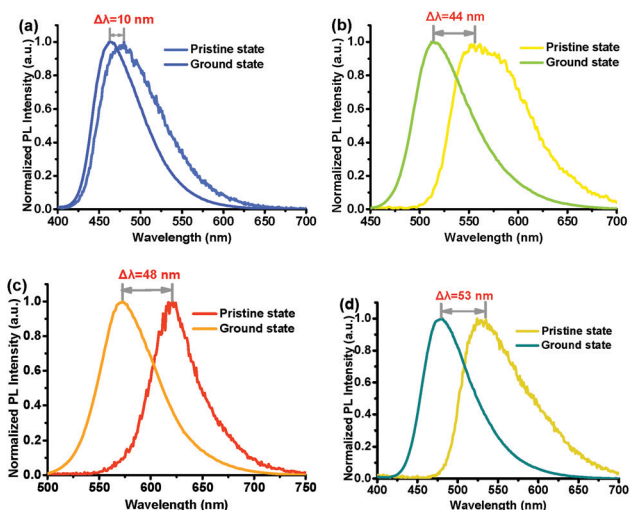


Fig. 5 Normalized emission spectra of the (a) APCz, (b) APAd, (c) APPo and (d) APpt samples before and after grinding.

the relatively low Φ_{F} s of the pristine powders of APCz, APAd, APPo, and APpt. After being ground, the sharp peaks were considerably diminished, indicating the amorphous characteristics of the ground samples. The principle of MRL behavior of APCz, APAd, APPo, and APpt can be attributed to the phase transformation from crystal state to amorphous state thus far.

As shown in Fig. 6e–h and Table 2, the fluorescence lifetimes of the ground states of APCz, APAd, APPo and APpt became longer than those in pristine powders, suggesting that phase transformation should occur upon mechanical grinding. The radiative rate constant (κ_{r}) of the ground samples increased by

as much as 12-, 33-, 11-, and 41-fold with respect to those of the pristine APCz, APAd, APPo, and APpt powders, respectively. Such increased κ_{r} s values indicated the activation of radiative pathways in the molecular arrangements of the ground samples, thereby accounting for the high Φ_{F} s of these samples.

Subsequently, deep insights from a molecular level to understand the structure–property relationship were obtained by a single-crystal XRD (SCXRD) study in deciphering diverse MRL contrast ratios of the luminophores. Fortunately, the good-quality crystals of APCz, APAd, and APPo with blue, bright yellow, and red luminescence were successfully cultured from the binary mixture of hexane:dichloromethane (1:1) at 25 °C (crystallographic data in detail are provided in Tables S1–S4, ESI†), respectively. However, the single crystal of APpt with considerable quality has not been obtained in our laboratory to satisfy the study. Considering the similar molecular structures between APPo and APpt, we believe that the information on the structure–property relationship would be deduced from the combination of DFT calculation and SCXRD studies.^{39,40}

Fig. 7a–c reveal the torsion angles between the central heterocycles and the adjacent phenyl rings of 29°/29°, 30°/22°, and 21°/21° for APCz, APAd, and APPo, respectively. These values were slightly smaller than those of the isolated molecules in the gas phase (calculated by the DFT study), thereby suggesting that their molecules required additional planar conformations to fit into the crystalline lattices. APCz was crystallized in a triclinic system with the space group $P\bar{1}$ ($a = 10.8799[7]$ Å, $b = 13.3532[8]$ Å, and $c = 17.0824[10]$ Å). The four types of intermolecular interactions with different quantities were detected between the APCz molecules, namely, C–H···O=C, C–H···C–H, and C–H··· π , and π ··· π , as shown in Fig. 7d. Considering the intermolecular interaction-assisted planar structure, APCz molecules formed interlaced herringbone patterns (Fig. 7g). In the case of APAd, each unit cell contained 16 molecules and belonged to a monoclinic system with the space group Cc ($a = 22.7890[12]$ Å, $b = 11.8841[7]$ Å, and $c = 38.1493[18]$ Å). Compared with crystal APCz, the types of noncovalent interactions in the crystal APAd were reduced, accompanied with the fluctuation in respective quantities (Table S4, ESI†). Three kinds of intermolecular interactions, including the largest quantity of C–H···O=C, medium quantity of C–H···C–H, and minimum quantity of C–H··· π were observed as the dominant driving forces in forming the face-to-face parallel pattern (Fig. 7e and h). The types of noncovalent interactions were further reduced in the crystal APPo, as shown in Fig. 7f. APPo crystallized in a monoclinic system with the space group $P21/m$ ($a = 9.3553[5]$ Å, $b = 25.1617[13]$ Å, and $c = 9.5973[5]$ Å).

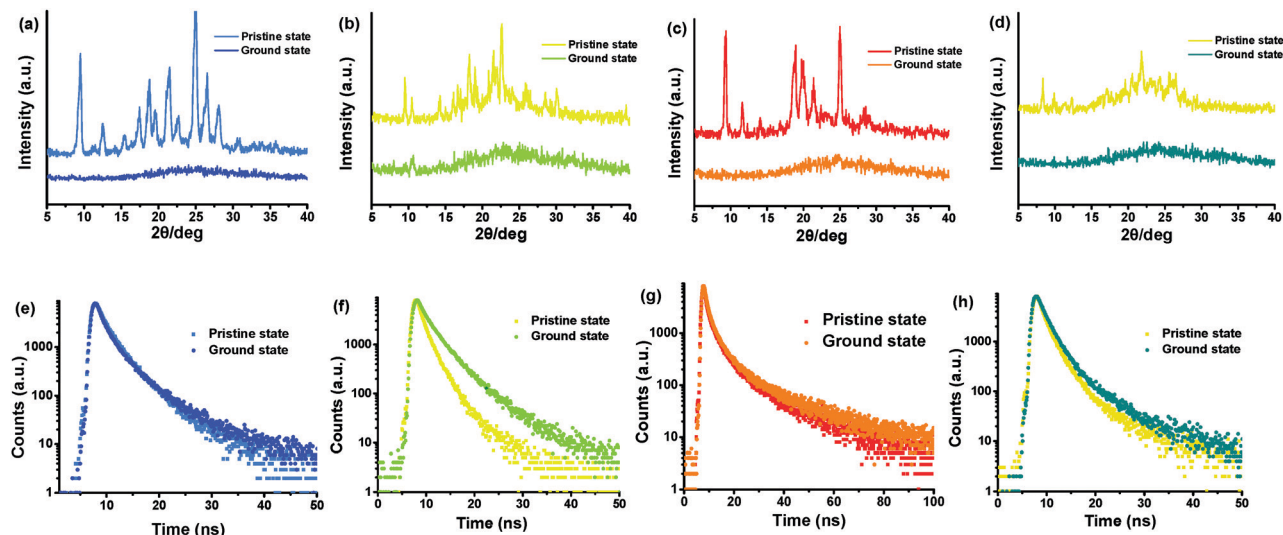


Fig. 6 XRD patterns of pristine and ground samples of (a) APCz, (b) APAd, (c) APPo and (d) APPr. Time-resolved fluorescence spectra of pristine and ground samples of (e) APCz, (f) APAd, (g) APPo and (h) APPr.

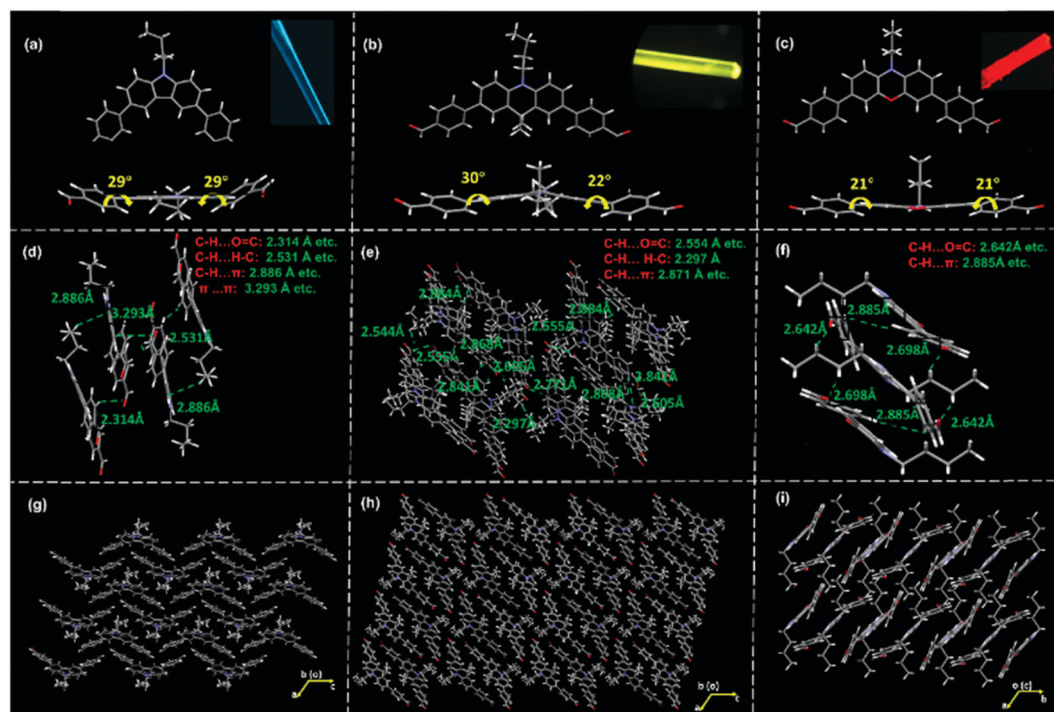


Fig. 7 Crystal structure of (a) APCz, (b) APAd and (c) APPo; multiple non-covalent interactions in the crystals of (d) APCz, (e) APAd and (f) APPo; different molecular packing modes of (g) APCz, (h) APAd and (i) APPo. Inset: The fluorescence microscopy images of single crystal APCz, APAd and APPo, respectively.

Each unit cell contained four molecules, which formed face-to-face parallel patterns under the interaction, namely $\text{C-H}\cdots\text{O}=\text{C}$ and $\text{C-H}\cdots\pi$, as shown in Fig. 7f and i. The category and quantity of noncovalent interactions were close to the compound-MRL contrast ratio. To provide a clear idea, we mapped the types *versus* the quantity of the noncovalent interactions in APCz, APAd, and APPo crystals, as well as compound-MRL contrast ratio correlation, as shown in Fig. 8 and Table S4 (ESI[†]). The MRL contrast ratio of the

compounds to the mechanical force increased with decreased types of noncovalent interactions, thereby exhibiting only a 10 nm spectral shift under mechanical stimuli. Meanwhile, APPo only possessed two types of noncovalent interactions, thereby resulting in a 48 nm spectral shift regardless of its quantities. Molecular conformation is another considerable parameter that influences the compound-MRL contrast ratio. Therefore, under the same condition, APPr

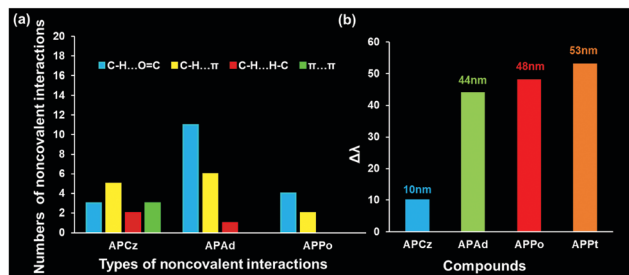


Fig. 8 (a) Types versus the quantity of the noncovalent interactions in APCz, APAd and APPo crystals; (b) compound-MRL contrast ratio correlation.

naturally exhibits the largest MRL contrast ratio among the samples due to its increased molecular distortion compared with that of APPo.

Conclusions

Insights into the molecular features regarding the structure–property relationship were obtained in designing MRL materials with high contrast ratios by carefully investigating the MRL behavior of the four simple heterocycle based aromatic aldehydes. Density functional theory and single-crystal analysis revealed that the features of the heterocycle at the core of symmetrical aromatic aldehydes significantly influenced the compounds' stability, molecular conformations, molecular-packing models, and intermolecular interactions, thereby regulating the MRL contrast ratio. The introduction of heterocyclic cores is responsible for the observed metastable states of APCz, APAd, APPo, and APPT in the pristine powders. Changing the heterocyclic cores from the five-membered rings to six-membered rings with additional heteroatoms decreased the types of noncovalent interactions, which subsequently increased the MRL contrast ratio of the compounds. Together with the appropriately increased molecular distortion, APPT exhibited the highest MRL contrast ratio (a spectral shift of 53 nm), accompanied by a remarkable change in fluorescence color and enhancement from yellow to blue. Our investigation provides a suggestion of the necessary features that a luminophore should possess in improving the MRL contrast ratio.

Conflicts of interest

There are no conflicts to declare.

Acknowledgements

This work was financially supported by the National Natural Science Foundation of China (61605138) and the Natural Science Foundation of Shanxi Province (201601D011031 and 201601D202030).

References

- 1 Y. Gong, G. Chen, Q. Peng, W. Z. Yuan, Y. Xie, S. Li, Y. Zhang and B. Z. Tang, *Adv. Mater.*, 2015, 27, 6195–6201.

- 2 B. Li, K. Seth, B. Niu, L. Pan, H. Yang and H. Ge, *Angew. Chem., Int. Ed.*, 2018, 57, 3401–3405.
- 3 Y. Qi, N. Ding, Z. Wang, L. Xu and Y. Fang, *ACS Appl. Mater. Interfaces*, 2019, 11, 8676–8684.
- 4 J.-C. Zhang, C. Pan, Y.-F. Zhu, L.-Z. Zhao, H.-W. He, X. Liu and J. Qiu, *Adv. Mater.*, 2018, 30, e1804644.
- 5 W. Zhao, Z. He, Q. Peng, J. W. Y. Lam, H. Ma, Z. Qiu, Y. Chen, Z. Zhao, Z. Shuai, Y. Dong and B. Z. Tang, *Nat. Commun.*, 2018, 9, 3044–3052.
- 6 D. A. Davis, A. Hamilton, J. Yang, L. D. Cremer, D. Van Gough, S. L. Potisek, M. T. Ong, P. V. Braun, T. J. Martinez, S. R. White, J. S. Moore and N. R. Sottos, *Nature*, 2009, 459, 68–72.
- 7 C. Wang, B. Xu, M. Li, Z. Chi, Y. Xie, Q. Li and Z. Li, *Mater. Horiz.*, 2016, 3, 220–225.
- 8 J. Wu, Y. Cheng, J. Lan, D. Wu, S. Qian, L. Yan, Z. He, X. Li, K. Wang, B. Zou and J. You, *J. Am. Chem. Soc.*, 2016, 138, 12803–12812.
- 9 Z. Chi, X. Zhang, B. Xu, X. Zhou, C. Ma, Y. Zhang, S. Liu and J. Xu, *Chem. Soc. Rev.*, 2012, 41, 3878–3896.
- 10 W. Yang, C. Liu, S. Lu, J. Du, Q. Gao, R. Zhang, Y. Liu and C. Yang, *J. Mater. Chem. C*, 2018, 6, 290–298.
- 11 Y. Zhang, Y.-Q. Feng, X.-X. Tian, J.-H. Wang, H. Li, G. Han and D. Li, *Adv. Opt. Mater.*, 2018, 6, 1800903.
- 12 S. Mo, Q. Meng, S. Wan, Z. Su, H. Yan, B. Z. Tang and M. Yin, *Adv. Funct. Mater.*, 2017, 27, 1701210.
- 13 J. Li, R. Zhang, Z. Wang, B. Zhao, J. Xie, F. Zhang, H. Wang and K. Guo, *Adv. Opt. Mater.*, 2018, 6, 1701256.
- 14 Y. G. Shi, J. W. Wang, H. Li, G. F. Hu, X. Li, S. K. Møllerup, N. Wang, T. Peng and S. Wang, *Chem. Sci.*, 2018, 9, 1902–1911.
- 15 T. Mutai, H. Satou and K. Araki, *Nat. Mater.*, 2005, 4, 685–687.
- 16 B. Roy, M. C. Reddy and P. Hazra, *Chem. Sci.*, 2018, 9, 3592–3606.
- 17 J. Mei, N. L. Leung, R. T. Kwok, J. W. Lam and B. Z. Tang, *Chem. Rev.*, 2015, 115, 11718–11940.
- 18 P. Xue, P. Chen, J. Jia, Q. Xu, J. Sun, B. Yao, Z. Zhang and R. Lu, *Chem. Commun.*, 2014, 50, 2569–2571.
- 19 Z. Xie, Q. Huang, T. Yu, L. Wang, Z. Mao, W. Li, Z. Yang, Y. Zhang, S. Liu, J. Xu, Z. Chi and M. P. Aldred, *Adv. Funct. Mater.*, 2017, 27, 1703918.
- 20 T. Jadhav, B. Dhokale and R. Misra, *J. Mater. Chem. C*, 2015, 3, 9063–9068.
- 21 Y. Qi, Y. Wang, G. Ge, Z. Liu, Y. Yu and M. Xue, *J. Mater. Chem. C*, 2017, 5, 11030–11038.
- 22 P.-Z. Chen, H. Zhang, L.-Y. Niu, Y. Zhang, Y.-Z. Chen, H.-B. Fu and Q.-Z. Yang, *Adv. Funct. Mater.*, 2017, 27, 1700332.
- 23 K. Guo, F. Zhang, S. Guo, K. Li, X. Lu, J. Li, H. Wang, J. Cheng and Q. Zhao, *Chem. Commun.*, 2017, 53, 1309–1312.
- 24 F. Zhang, R. Zhang, X. Liang, K. Guo, Z. Han, X. Lu, J. Xie, J. Li, D. Li and X. Tian, *Dyes Pigm.*, 2018, 155, 225–232.
- 25 Y. Guo, L. Xu, H. Liu, Y. Li, C. M. Che and Y. Li, *Adv. Mater.*, 2015, 27, 985–1013.
- 26 A. Li, Z. Ma, J. Wu, P. Li, H. Wang, Y. Geng, S. Xu, B. Yang, H. Zhang, H. Cui and W. Xu, *Adv. Opt. Mater.*, 2018, 6, 1700647.

- 27 S. Biswas, D. Jana, G. S. Kumar, S. Maji, P. Kundu, U. K. Ghorai, R. P. Giri, B. Das, N. Chattopadhyay, B. K. Ghorai and S. Acharya, *ACS Appl. Mater. Interfaces*, 2018, **10**, 17409–17418.
- 28 D.-Y. Kim, J. Koo, S.-I. Lim and K.-U. Jeong, *Adv. Funct. Mater.*, 2018, **28**, 1707075.
- 29 Q. Zhu, K. Van Vliet, N. Holten-Andersen and A. Miserez, *Adv. Funct. Mater.*, 2019, **29**, 1808191.
- 30 T. Seki, Y. Takamatsu and H. Ito, *J. Am. Chem. Soc.*, 2016, **138**, 6252–6260.
- 31 Y. Hong, J. W. Y. Lam and B. Z. Tang, *Chem. Commun.*, 2009, 4332–4353.
- 32 A. Deak, C. Jobbagy, G. Marsi, M. Molnar, Z. Szakacs and P. Baranyai, *Chemistry*, 2015, **21**, 11495–11508.
- 33 K. Suenaga, K. Tanaka and Y. Chujo, *Chemistry*, 2017, **23**, 1409–1414.
- 34 Y. Sagara, M. Karman, E. Verde-Sesto, K. Matsuo, Y. Kim, N. Tamaoki and C. Weder, *J. Am. Chem. Soc.*, 2018, **140**, 1584–1587.
- 35 S. Tong, S. Zhao, Q. He, Q. Wang, M. X. Wang and J. Zhu, *Angew. Chem., Int. Ed.*, 2017, **56**, 6599–6603.
- 36 P. Wen, Z. Gao, R. Zhang, A. Li, F. Zhang, J. Li, J. Xie, Y. Wu, M. Wu and K. Guo, *J. Mater. Chem. C*, 2017, **5**, 6136–6144.
- 37 Y. Zhang, H. Li, G. Zhang, X. Xu, L. Kong, X. Tao, Y. Tian and J. Yang, *J. Mater. Chem. C*, 2016, **4**, 2971–2978.
- 38 Z. Wang, Z. Peng, K. Huang, P. Lu and Y. Wang, *J. Mater. Chem. C*, 2019, **7**, 6706–6713.
- 39 M. Okazaki, Y. Takeda, P. Data, P. Pander, H. Higginbotham, A. P. Monkman and S. Minakata, *Chem. Sci.*, 2017, **8**, 2677–2686.
- 40 J. Yang, J. Qin, P. Geng, J. Wang, M. Fang and Z. Li, *Angew. Chem., Int. Ed.*, 2018, **57**, 14174–14178.